Structural Monitoring and Maintenance, *Vol. 5, No. 2 (2018) 189-204*
DOI: https:// doi.org/10.12989/smm.2018.5.2.189

Seismic response analysis of RC frame core-tube building with self-centering braces

Long-He Xu*, Shui-Jing Xiao[a] and Xiao Lu[b]

School of Civil Engineering, Beijing Jiaotong University, Beijing 100044, China

(Received February 23, 2018, Revised March 29, 2018, Accepted March 30, 2018)

Abstract. This paper examines the seismic responses of a reinforced concrete (RC) frame core-tube building with pre-pressed spring self-centering energy dissipation (PS-SCED) braces. The PS-SCED brace system consists of friction devices for energy dissipation, pre-pressed combination disc springs for self-centering and tube members as guiding elements. A constitutive model of self-centering flag-shaped hysteresis for PS-SCED brace is developed to better simulate the seismic responses of the RC frame core-tube building with PS-SCED braces, which is also verified by the tests of two braces under low cyclic reversed loading. Results indicate that the self-centering and energy dissipation capabilities are well predicted by the proposed constitutive model of the PS-SCED brace. The structure with PS-SCED braces presents similar peak story drift ratio, smaller peak acceleration, smaller base shear force and much smaller residual deformations as compared to the RC frame core-tube building with bucking-restrained braces (BRBs).

Keywords: RC frame core-tube building; PS-SCED brace; constitutive model; seismic performance; self-centering capability; residual deformation

1. Introduction

Although the traditional structural systems designed and constructed according to current seismic design codes can provide adequate safety to avoid structural collapse during earthquakes, they are likely to produce concentrated damage through repeated inelastic actions as well as residual deformations which can seriously damage the structure and increase repair costs after strong earthquakes. For instance, the lateral stiffness and strength of the RC frame core-tube building are greatly improved by the core-tube, and the seismic performance under low- and medium-level earthquakes is also greatly enhanced. However, the damage concentrated on the shear walls and the residual deformation of the structure is significant under strong earthquakes, which can result in substantial costs or an undesirable potential collapse hazard (Lu *et al*. 2013). Therefore, the resilience-based earthquake design for buildings has become an important trend in earthquake engineering (Deierlein *et al*. 2011, Mayes *et al*. 2012, Lu *et al*. 2013, Takewaki *et al*.

*Corresponding author, Professor, E-mail: lhxu@bjtu.edu.cn
[a] Ph.D. Candidate, E-mail: 14121117@bjtu.edu.cn
[b] Associate professor, E-mail: xiaolu@bjtu.edu.cn

http://www.techno-press.org/?journal=smm&subpage=7 ISSN: 2288-6605 (Print), 2288-6613 (Online)

2012).

Residual deformations should be considered in a performance-based design procedure for the earthquake-resilient structures (Christopoulos *et al*. 2003, Pampanin *et al*. 2003, Wu *et al*. 2004). They can also be reduced or completely eliminated by using systems with self-centering capability, such as those exhibiting flag-shaped hysteretic responses. Various earthquake-resilient systems with self-centering capability had been proposed and verified by experiments (Lu *et al*. 2017, Liu and Jiang 2017). For instance, a rocking system allows columns or walls to uplift at its bases during strong earthquakes, and the restoring force is provided by gravity or pre-stress elements (Hitaka and Sakini 2008, Wada *et al*. 2009). Eatherton *et al*. (2010) proposed a controlled rocking system which comprised of vertical post-tensioning and energy dissipation fuses, and the test results indicated that the rocking system can sustain rare earthquakes with minimal damage and even eliminate the residual deformation after earthquakes. Furthermore, the self-centering braced systems were also widely investigated by researchers in recent years (Chou *et al*. 2014, Chou and Chen 2015, Steele and Wiebe 2017). Miller *et al*. (2011, 2012) proposed a new type of self-centering buckling-restrained brace (SC-BRB) that used shape memory alloy (SMA) bars to provide restoring force and a BRB component to dissipate energy. Erochko *et al*. (2010) proposed an enhanced-elongation telescoping self-centering energy dissipation (T-SCED) brace to overcome the limited deformation capacity of the original SCED brace resulting from the elongation capacity of the tendons. Dynamic tests on a full-scale vertical steel frame demonstrated that more than twice the original deformation range can be accommodated by the T-SCED brace. Xu *et al*. (2016a, b, c, 2017) proposed a novel self-centering brace configuration, in which the friction devices were used for energy dissipation in the proposed pre-pressed spring self-centering energy dissipation (PS-SCED) brace, while a pre-pressed disc spring mechanism instead of tendons or SMA bars was employed to provide the self-centering capability. Comparative studies of SDOF systems by Christopoulos *et al*. (2008) and Tremblay *et al*. (2008) showed that these self-centering braced systems matched or improved the response of equivalent elastic-plastic braced systems in terms of displacement demand without residual drift when sufficient energy dissipation capacity was provided.

In this paper, a novel PS-SCED brace is designed and applied to the RC frame core-tube building. The PS-SCED brace consists of friction devices for energy dissipation, pre-pressed combination disc springs for self-centering and tube members as guiding elements. A series of quasi-static tests were conducted to evaluate the hysteretic behaviors of the PS-SCED brace. To better simulate the hysteretic behavior of PS-SCED brace in the RC frame core-tube structure, a constitutive model of self-centering flag-shaped hysteresis for PS-SCED brace is developed. The constitutive model is verified by the tests of two braces under low cyclic reversed loading, and which is used to further study the seismic performance of the RC frame core-tube building with PS-SCED braces under ground motion ensembles corresponding to two hazard levels (frequent earthquake and rare earthquake). Furthermore, the identical building equipped with BRBs is also simulated for comparison, and several response parameters are studied to compare the behavior of the two bracing systems.

2. Configuration and mechanical model of PS-SCED brace

2.1 Configuration of PS-SCED *brace*

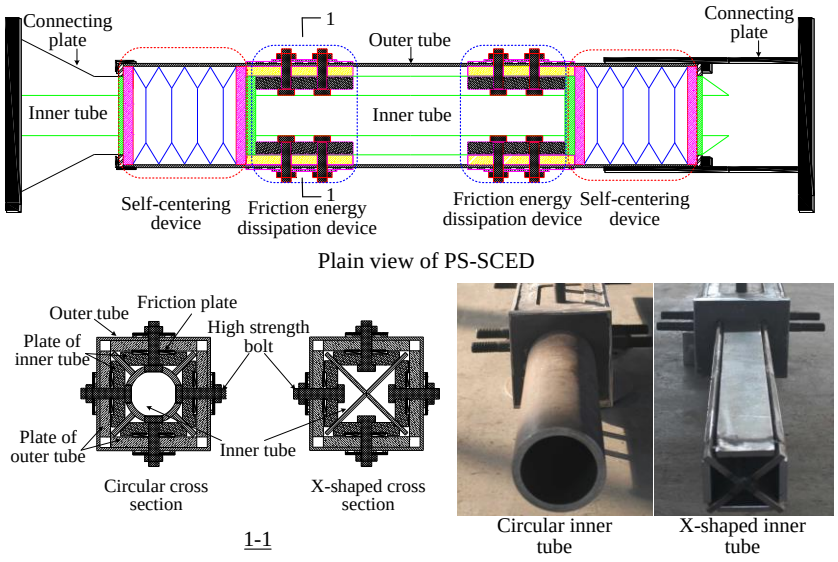

Fig. 1 Configuration of PS-SCED brace

The PS-SCED brace is composed of three main parts, the friction devices for energy dissipation, the self-centering devices and the guiding element members including the inner tube, the outer tube, the connecting plates and several blocking plates, as shown in Fig. 1. The energy dissipation devices employ the friction pads capable of exerting a stable energy dissipation capability. The circular or X-shaped inner tube is introduced into the welding plates and combination disc springs, the friction pads are installed at the plates between the inner and outer tube around four sides and the high strength bolts are used to apply the normal force, as shown in Fig. 1. The friction devices are activated by the relative movement induced between the inner and outer tubes. Compared to the original SCED brace that employed the tendons or SMA bars to provide the restoring force, it is easier to assemble the pre-pressed disc springs on the inner tube, and the deformation demand is better achieved by installing the combination disc springs in series. The combination disc springs are pre-pressed at an initial state, and the restoring force increases as the PS-SCED brace deforms axially. All steel members of the PS-SCED brace are designed to remain elastic so that all the energy is dissipated by the external friction devices.

Fig. 2 presents the theoretical hysteretic response of the PS-SCED brace that combined two self-centering devices installed at both ends of the bracing component with two friction devices installed at the middle of the bracing system. The mechanical responses of the brace can be divided into four stages of stretching and compression. When the brace is compressed, the inner and outer tubes are first pressed without sliding and the bracing system exhibits a higher initial stiffness, K_1, determined by the sum of the stiffness of the inner and outer tubes, as shown in Fig. 2. The relative movement occurs between the inner and outer tubes when the external force is larger than the sum of the friction F_0 and the initial pre-pressed force P_0, and the stiffness of the bracing system is K_2 at the second stage, which is provided by the combination disc springs of the two self-centering devices. When the external force is reversed, the friction induced by the friction device is also reversed and the relative movement between the inner and outer tubes stops, the

stiffness of the bracing system is still K_1 at the third stage. After the external force reduces by $2F_0$, the inner and outer tubes are pulled back to their initial positions by the restoring force provided by the compressed disc springs, and the stiffness of the bracing system is also K_2. The behaviors of the bracing system in tension are the same as one in compression, as shown in Fig. 2. Full self-centering capability can be achieved by providing adequate initial pre-pressed force to overcome the friction force, and the inner and outer tubes can return to their initial positions with no residual deformations.

To validate the hysteretic behavior of the PS-SCED brace, a series of low cyclic reversed loading tests were conducted using the 3000 kN servo hydraulic test system by Xu *et al*. (2016a, b, c, 2017, 2018a, b), as shown in Fig. 3. Two brace specimens, brace I with the circular cross section inner tube and brace II with the X-shaped cross section inner tube, were tested. The initial pre-pressed force was set to 270 kN and all the bolts of the friction devices were subsequently stressed to provide friction force of 200 kN and 300 kN for both braces. The loading scheme of the two braces is shown in Fig. 4, which employed a displacement-control loading scheme with three cycles at each target displacement.

The hysteretic responses of the tested PS-SCED brace I and brace II are shown in Fig. 5 and Fig. 6, respectively.

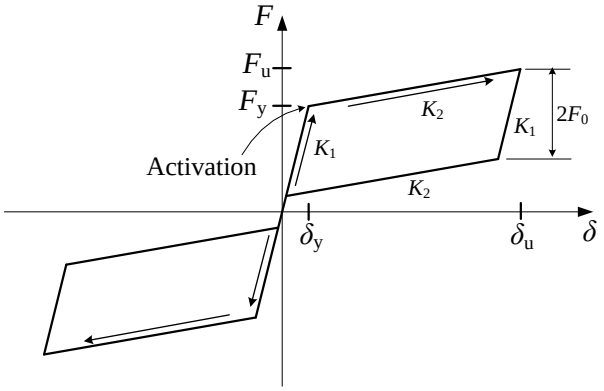

Fig.2 Theoretical hysteretic response of the PS-SCED brace

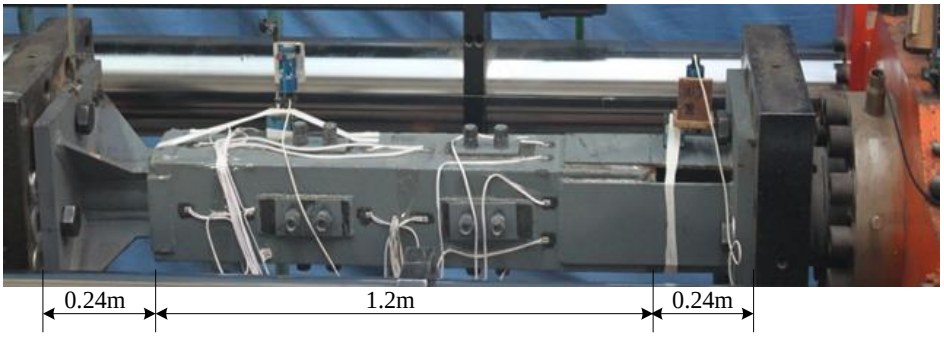

Fig. 3 Test setup of the PS-SCED brace

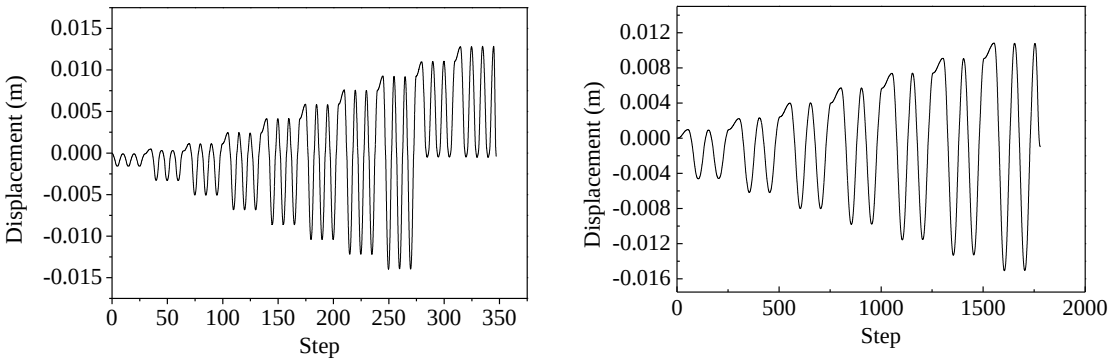

(a) Brace I (b) Brace II

Fig. 4 Loading scheme of PS-SCED braces

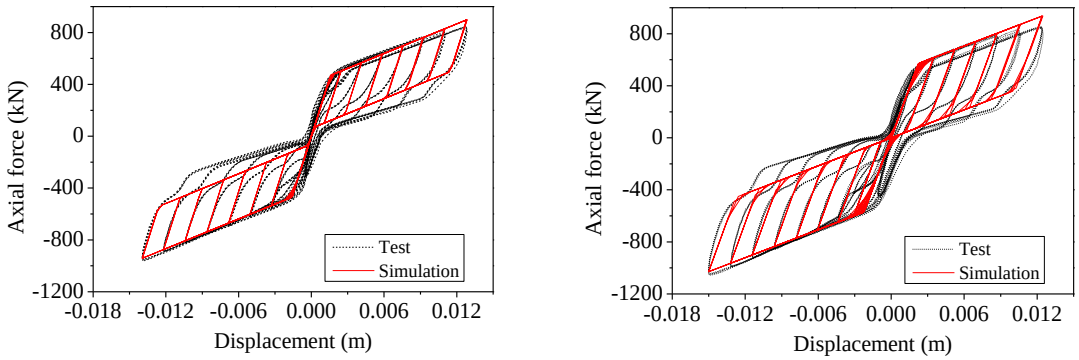

(a) 200 kN (b) 300 kN

Fig. 5 Hysteretic curves of PS-SCED brace I with different friction

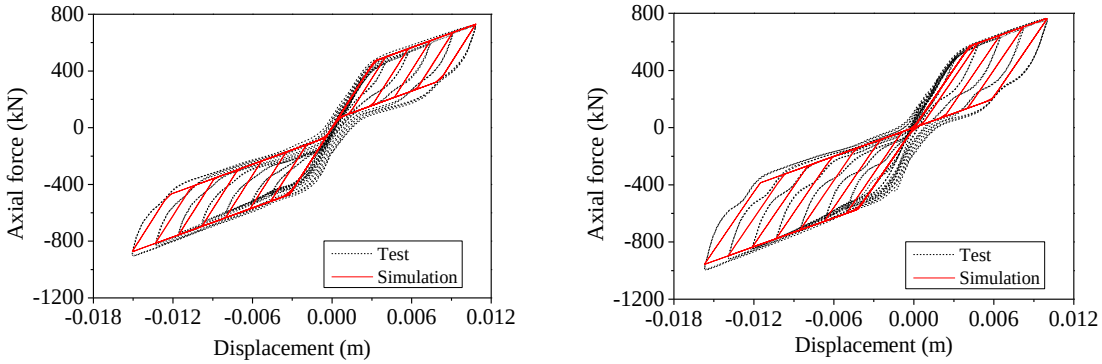

(a) 200 kN (b) 300 kN

Fig. 6 Hysteretic curves of PS-SCED brace II with different friction

Because the servo hydraulic test system produced unsymmetrical loading displacement in compression and tension, several cycles in tension were added to achieve the equivalent maximum displacement of the brace during the tests. It is observed that both the brace I and brace II exhibit the stable flag-shaped hysteretic responses. Almost no residual deformation is observed when the friction force is less than the pre-pressed force, as shown in Figs. 5(a) and 6(a), while obvious residual deformation is observed when the friction force is larger than the pre-pressed force, as shown in Figs. 5(b) and 6(b). Good energy dissipation capability is also observed, and the PS-SCED brace with larger friction force has better energy dissipation capability. Furthermore, the bearing capacity of the PS-SCED brace I is larger than that of the brace II.

2.2 Constitutive model of PS-SCED *brace*

In order to better study the performance of the structure, a constitutive model of the PS-SCED brace is developed by using the computer program MSC.Marc. The relationship between force and displacement is defined directly by the spring element to describe the flag-shaped hysteric response of the PS-SCED brace. The mechanical behavior of the PS-SCED brace is divided into four stages of stretching and compression, as show in Fig. 2. Four parameters, the initial stiffness K_1 of the inner and outer tubes, the stiffness K_2 of combination disc springs, the friction force F_0 and the initial pre-pressed force P_0 are defined to control the relationship between force and displacement of the PS-SCED brace under the external loads. The four parameters are determined by the size and material of the designed PS-SCED brace.

The hysteretic behaviors of the tested PS-SCED braces are simulated by the developed constitutive model, and the comparison results are shown in Figs. 5 and 6, respectively. It is observed that stable self-centering and energy dissipation capabilities are obtained, and the bearing capacities of the two braces are well simulated by the developed constitutive model at each target loading displacement. Table 1 shows the experimental and simulated bearing capacities of brace I and brace II with different frictions corresponding to various deformation ratios. The bearing capacity is calculated from the average compressive and tensile bearing forces and the deformation ratio is the ratio of the loading displacement to the length of the specimen. It is observed that the maximum errors between tests and simulation of brace I with F_0=200 kN and F_0=300 kN are 3.1% and 4.1%, respectively, and of brace II with F_0=200 kN and F_0=300 kN are 4.7% and 7.7%, respectively, which indicate that the hysteretic responses of brace I and brace II are accurately predicted by the proposed constitutive model. However, differences in the residual deformation and unloading force of brace I at the fourth stage can be found after the load is removed. Table 2 lists the experimental and simulated equivalent viscous damping ratios at the maximum displacement $\Delta_{\max}$ of the two braces. It is observed that the energy dissipation capability of brace I is underestimated by the developed constitutive model, with a maximum error of 24.98%. This is mainly due to the ideal assumption that the stiffness K_4 equals K_2 in the proposed constitutive model, and the friction among all members of the test brace specimens may also cause some differences. While the differences of brace II are smaller, it demonstrates that the behaviors of the PS-SCED brace are greatly affected by the cross-sectional form of the inner tube. Overall, the proposed constitutive model can be used to simulate the experimental mechanical behaviors of the PS-SCED brace, which can also be used to simulate the behavior of the braces in the structure to further evaluate the earthquake-resilient performance of structure.

Table 1 Experimental and simulated bearing capacities of brace I and brace II

Deformation ratios (%)	Bearing capacity of brace I (kN)				Bearing capacity of brace II (kN)			
	F_0=200 kN		F_0=300 kN		F_0=200 kN		F_0=300 kN	
	Test	Simulation	Test	Simulation	Test	Simulation	Test	Simulation
0.1	487.02	470.84	544.26	567.55	454.44	470.40	522.63	566.45
0.3	612.88	599.80	659.48	675.77	507.84	532.21	565.01	589.09
0.5	741.52	731.31	794.23	798.03	606.51	622.17	627.40	648.87
0.7	833.13	844.31	874	882.93	698.49	707.77	696.47	707.20
0.8	868.57	885.49	919.33	951.25	773.07	771.04	766.69	768.14
0.9	956.76	940.16	1044.86	1024.43	899.94	870.34	998.03	949.85
Maximum error (%)	3.3		4.1		4.7		7.7	

Table 2 Experimental and simulated equivalent viscous damping ratios at maximum displacements of braces

Maximum displacement	Equivalent viscous damping ratio of brace I				Equivalent viscous damping ratio of brace II			
	F_0=200 kN		F_0=300 kN		F_0=200 kN		F_0=300 kN	
	Test	Simulation	Test	Simulation	Test	Simulation	Test	Simulation
Δ_{max}	14.88	13.44	14.78	12.26	8.63	10.11	13.84	12.53
$-\Delta_{max}$	14.68	13.23	16.73	12.55	10.07	10.13	13.39	12.57
Maximum error (%)	9.88		24.98		14.64		9.5	

3. Prototype building and numerical modelling

3.1 Parameters of the prototype building

Fig. 7 shows the plan view of the prototype RC frame core-tube building. This 13-story building is 97.2 m × 34.8 m in plan and 61.2 m in elevation including the roof height, and has two RC core-tubes in plan. The height of the first floor is 5.7 m, and that of other floors is 4.3 m. The building was built in China in a high risk seismic region. The basic seismic acceleration is 0.2 g, the characteristic period of the ground motion is 0.45 s, and the damping ratio is 0.05 of the structure. The BRBs or PS-SCED braces are installed at four bays of the structure, as shown in Fig. 7. The front view of the analytical models with braces are shown in Fig. 8, in which a two-bay chevron bracing configuration is selected for the structure with BRBs or PS-SCED braces. Each RC core-tube is 24.3 m×11.4 m rectangle, and the concrete compressive strengths of the core-tube and RC columns are 32.4 MPa at the lower 10 stories and 26.8 MPa at the upper 3 stories, respectively. For the concrete beams and floors, the concrete compressive strengths are 26.8 MPa at the lower 10 stories and 20.1 MPa at the upper 3 stories, respectively. The yield strength of the brace and the steel plate embedded in the column, beam and shear wall is 235 MPa. The yield strength of longitudinal reinforcement and stirrup is 400MPa and 300MPa, respectively.

For the PS-SCED braced structure, the dimensions of the components are the same as those of the designed structure with BRBs. Only the parameters and the mechanical model of the two braces are different, as shown in Fig. 8.

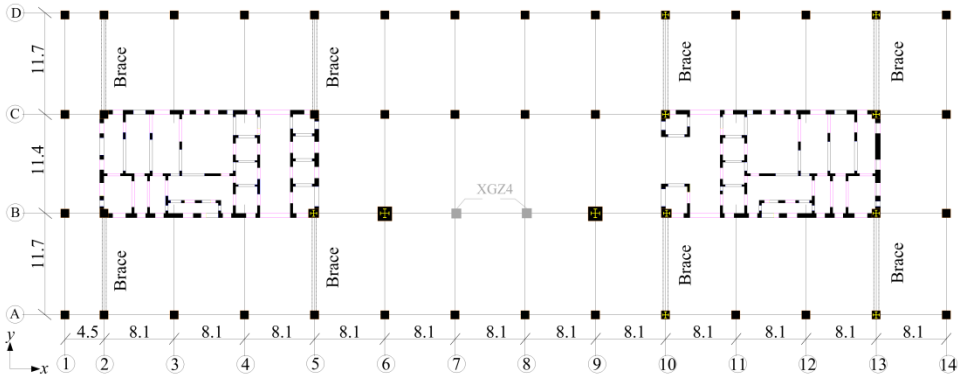

Fig. 7 Plan view of the frame core-tube building

Table 3 Design parameters of BRBs and PS-SCED braces in two buildings

BRBs	Yielding strength ($\times 10^3$ N)	PS-SCED braces	K_1 ($\times 10^6$ N/m)	K_2 ($\times 10^6$ N/m)	F_0 ($\times 10^3$ N)	F_f ($\times 10^3$ N)
BRB1	6600	PS-SCED-1	1120.1	28.7	4849	4388
BRB2	2300	PS-SCED-2	389.6	9.98	1690	1529
BRB3	900	PS-SCED-3	152.2	3.91	661	598
BRB4	900	PS-SCED-4	152.2	3.91	661	598

For the BRB, the cross-sectional area of the brace core is determined to develop a design axial strength which equals the required yield strength of the brace, and the effective cross-sectional area of the analytical model is equal to 1.48 (Tremblay *et al*. 2008) times the cross-sectional area of the brace core, which considers the strength of connecting plates. For the PS-SCED brace, the sliding force resulting in relative movement between the inner and outer tubes is designed to equal the yield strength of the BRB, and the ultimate bearing capacity corresponding to the deformation that reaches 2% of the inter-story displacement is designed to equal the ultimate bearing force of the BRB. The design parameters of BRBs and PS-SCED braces in two buildings are show in Table 3.

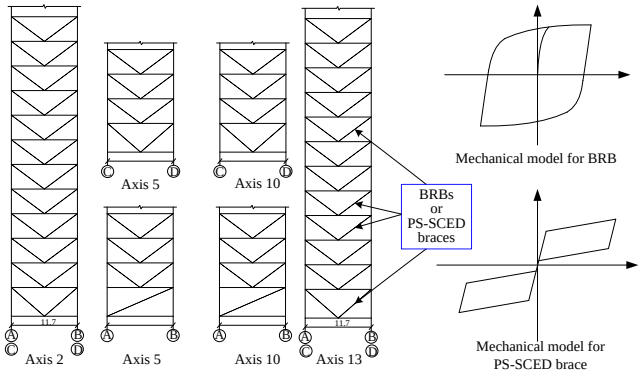

Fig. 8 Front view of the analysis models with braces

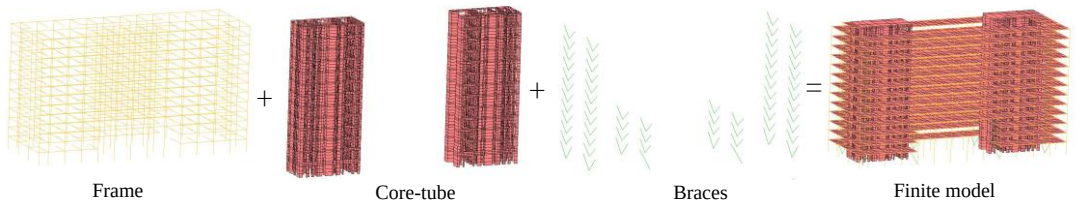

Fig. 9 Finite model of the frame core-tube structure

3.2 Modelling of two braced frame core-tube structures

Based on the general finite element program MSC.Marc, the 3D finite element (FE) models of the two frame core-tube structures are constructed by using the proposed material constitutive laws and element models, as shown in Fig. 9. The fiber-beam elements and multi-layer shell elements, which have been successfully used in some high-rise building dynamic simulation, are adopted in the FE models. In the fiber-beam element, the cross section of the beams or columns is divided into a number of fibers and each fiber exhibits different constitutive material model. In the multi-layer shell element, each element is divided into a number of layers along the thickness direction, and the horizontal and vertical reinforcement or the embedded steel plate of the wall are treated as the equivalent steel layers. Four types of constitutive material models are adopted in this analysis, including the elasto-plastic-fracture concrete constitutive models for the shear walls and coupling beams, the confined concrete constitutive model for the steel columns and beams, the elasto-plastic steel constitutive law for the steel reinforcement and steel tubes, and the developed flag-shaped hysteric model for the PS-SCED braces.

The shear walls and coupling beams in the core tubes are modeled by the multi-layer shell elements, which are divided into several layers with different steel and concrete materials, respectively. The applicability of this elasto-plastic-fracture concrete constitutive model is validated by Miao *et al*. (2011) and the numerical results agree well with the experimental data in simulating the mechanical behavior of RC members under complex stress states. According to the actual reinforcement arrangement in the shear wall, a total of ten layers are adopted in the multi-layer shell element. The FE models of the typical core tubes along the height of the building are shown in Fig. 10.

The steel columns and beams in the frame are simulated using fiber-beam elements, in which the fibers are defined by the different steel and concrete materials, respectively. The fiber distribution of the column and beam sections is shown in Fig. 11, in which the concrete fibers and steel fibers are 36 and 16, respectively. The confined concrete constitutive model proposed by Han *et al*. (2001) is adopted for the middle concrete fibers, as shown in Fig. 11. In addition, the steel plate in the column is modeled by a beam element with a closed section and connected to the column through a common node. The plastic constitutive model based on the von Mises yield criterion is used for steel material, and the stress-strain backbone curve exhibits four stages of elasticity, yielding, hardening and post-necking.

The BRBs in the frame are modeled by the beam elements with closed sections and each segment of the cross section (i.e., the flange and wed) is divided into 9 fibers to ensure the computation accuracy. The PS-SCED braces are simulated by the spring elements with the proposed flag-shaped hysteric model.

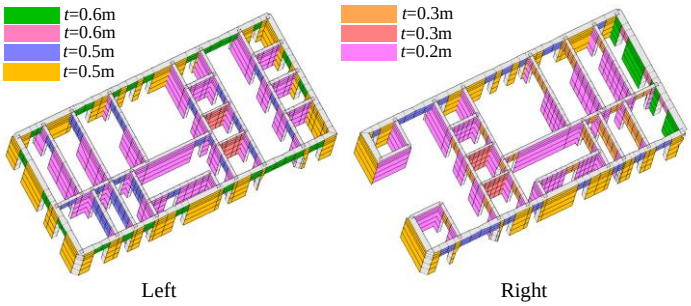

Fig. 10 FE models of typical core-tubes

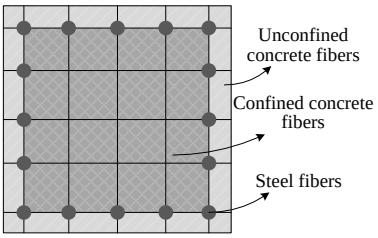

Fig. 11 Fiber distribution of the column and beam sections

4. Dynamic time history analyses

To obtain the basic dynamic properties of these two frame core-tube buildings with braces, a modal analysis is performed before the dynamic time history analyses. To be consistent with the design assumptions, the gravity loads corresponding to 1.0 times the dead load plus 0.5 times the live load are applied prior to starting the dynamic modal analysis, and *P*-delta effects are also considered through large displacement analysis. Initial Rayleigh damping ratio is considered as 5% for the concrete structure. It is noted that zero stiffness damping is assigned to the spring elements in simulating the slippage mechanisms in PS-SCED brace members to avoid the development of unrealistic damping forces when these mechanisms are activated.

The first six natural vibration periods of the two structures are shown in Table 4. It is observed that the fundamental periods of the two buildings are similar, and the first three corresponding modal shapes of the two buildings are shown in Figs. 12 and 13, respectively, which are the first translation in Y-direction, the second translation in X-direction and the third torsion of both structures with the BRBs and PS-SCED braces.

Table 4 The first six natural vibration periods of two frame core-tube buildings with braces

	Structure	T_1	T_2	T_3	T_4	T_5	T_6
Period (s)	BRB	1.047	1.01	0.94	0.43	0.43	0.43
	PS-SCED	1.045	1.01	0.93	0.35	0.35	0.34

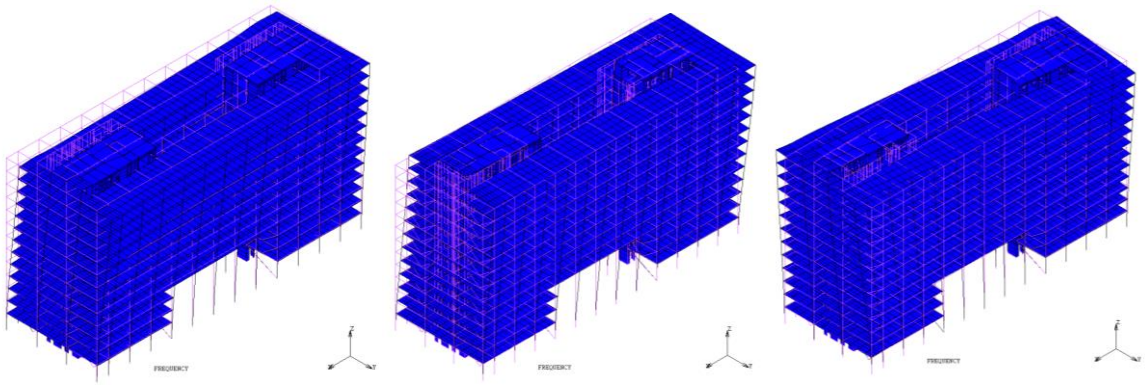

(a) The first-order translation in Y-direction (b) The first-order translation in X-direction (c) The first-order torsion

Fig. 12 The first three natural vibration modes of the RC frame core-tube building with BRBs

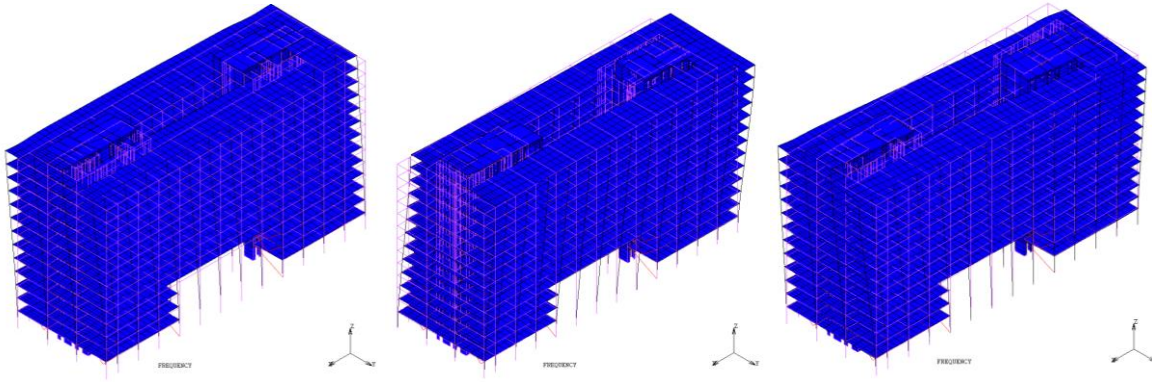

(a) The first-order translation in Y-direction (b) The first-order translation in X-direction (c) The first-order torsion

Fig. 13 The first three natural vibration modes of the RC frame core-tube building with PS-SCED braces

The ground motion recorded at the EL-Centro station in the USA in 1940s is selected as the excitation and applied to Y-direction of the buildings. The peak ground acceleration (PGA) is scaled to 70 cm/s^2 and 600 cm/s^2, respectively, to compare the seismic performance of these two buildings under earthquakes. Furthermore, the ground motion input is padded with zeros for 5 seconds to allow for free vibration decay and, hence, correctly capture the structural residual deformations. Four main parameters, the story displacement, the inter-story drift ratio, the peak absolute floor acceleration and the residual displacement of structures, are examined to evaluate the seismic performance of these two structures.

Comparisons of simulation results between the structures with the BRBs and the PS-SCED braces due to the El-Centro earthquake with PGA of 70 cm/s^2 are shown in Fig. 14. It is observed that the story displacement increases with the height of both two buildings, and the story displacement envelopes are corresponding to the deformation rule of the frame core-tube structure,

as shown in Fig. 14(a). The maximum inter-story drift ratio occurs at the forth story of both two buildings, as shown in Fig. 14(b), which is still less than the elastic inter-story drift ratio limit value of 0.0125. The comparison results among the story displacement envelopes (Fig. 14(a)), the story drift ratio envelopes (Fig. 14(b)) and the roof acceleration (Fig. 14(c)) indicate that the seismic responses of structures with the BRBs and PS-SCED braces are similar due to the similar initial stiffness of the two braces and the elastic deformation of components in the structures under the El-Centro earthquake with PGA of 70 cm/s^2. Furthermore, the BRBs and PS-SCED braces are also in elastic states.

To better study the nonlinear behaviors of the two structures, the simulations of them due to the El-Centro earthquake with PGA of 600 cm/s^2 are also conducted. The comparisons of the story displacement envelopes, the story drift ratio envelopes, the roof acceleration and the base shear force between the structures with BRBs and PS-SCED braces are shown in Fig. 15. Both structures are found to undergo large lateral deformations, and the maximum roof displacement exceeds $0.05h_s$, h_s is the story height. In addition, the maximum deformation at each story of both structures are similar, as shown in Fig. 15(a). The inter-story drift ratios of the structure with BRBs is smaller than that with PS-SCED braces from the ninth story to the twelfth story, as shown in Fig. 15(b), which is still less than the elastic-plastic inter-story drift ratio limit value of 0.01 mainly due to the effect of the double core tubes in plan. Fig. 15(c) compares the roof acceleration time history of the two structures due to the El-Centro earthquake with PGA of 600 cm/s^2. It is observed that the maximum acceleration occurs at approximately 2.0s, and the value of the frame core-tube structure with PS-SCED braces is smaller than that of the structure with BRBs. Fig. 15(d) shows the base shear force responses of the two buildings. Both buildings experience similar base shear force responses during the loading time, which can be explained by the fact that both the two braces display similar backbone load-deformation characteristics. The maximum base shear force of the building with PS-SCED braces occurs at approximately 5.0s, which is also slightly smaller than that of the structure with BRBs, which can reduce the damage to buildings with PS-SCED braces. The seismic responses of the structure with PS-SCED braces is similar to or even smaller than that of structure with BRBs, as shown in Figs. 15(c) and 15(d), which indicates that the structure with PS-SCED braces is useful to improve the seismic performance of structures under earthquakes.

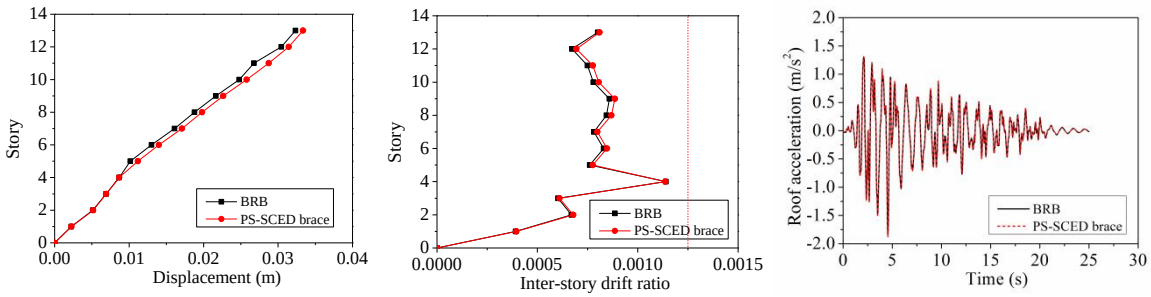

(a) Story displacement envelopes (b) Inter-story drift ratio envelopes (c) Roof acceleration time history

Fig. 14 Comparisons of simulation results between the structures with BRBs and PS-SCED braces due to the El-Centro earthquake with PGA of 70cm/s^2

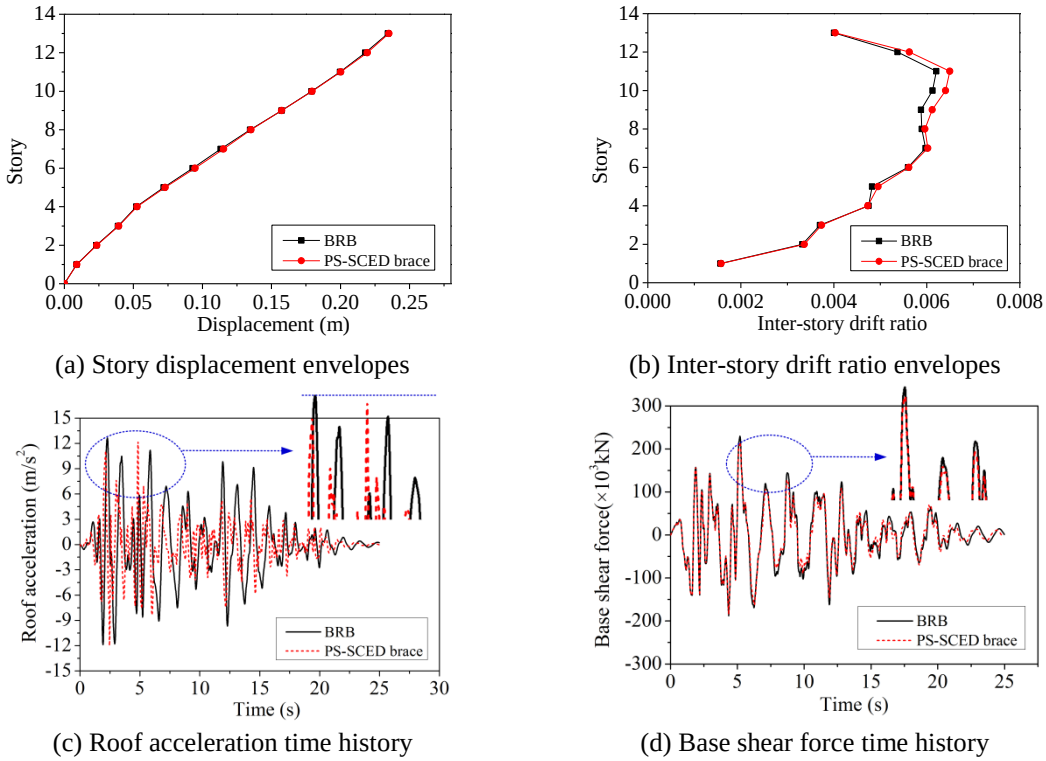

(a) Story displacement envelopes

(b) Inter-story drift ratio envelopes

(c) Roof acceleration time history

(d) Base shear force time history

Fig. 15 Comparisons of simulation results between the structures with BRBs and PS-SCED braces due to the El-Centro earthquake with PGA of 600cm/s^2

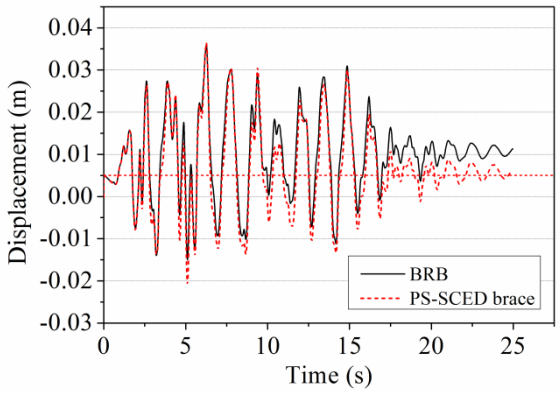

Fig. 16 Displacements time history at the forth story of structures with BRBs or PS-SCED braces

Fig. 16 shows the comparisons of the lateral displacements time history at the forth story of two frame core-tube structures due to the El-Centro earthquake with PGA of 600 cm/s^2. The two braced systems have similar peak deformations during the first 5 s due to similar backbone load-deformation characteristics of the BRBs and PS-SCED braces. After that, the plastic deformation of BRBs increase, and the peak deformations of the BRB structure are smaller than

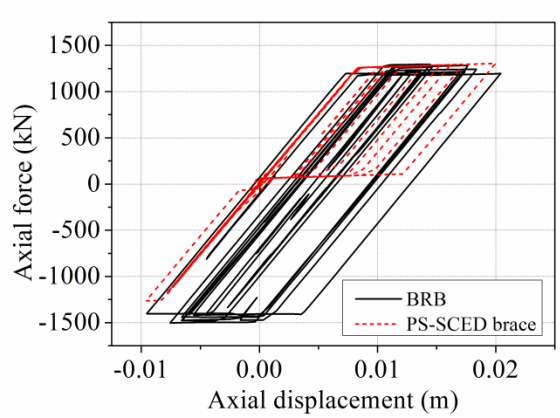

Fig. 17 Hysteretic responses of the two braces at the forth story of structure

that of the structure with PS-SCED braces. However, the response of the PS-SCED braced structure is characterized by several oscillations about the zero deformation position with no residual deformations at the end under earthquake. For the structure with BRBs, the hysteretic energy dissipation capacity of the BRBs is larger, resulting in a smaller displacement response and a deviation from the initial undeformed structure. The residual deformation ratio, denote as the ratio of residual deformation to the story height, has reached 0.3% for the structure with BRBs, which is hard to repair after earthquakes (Henry *et al*. 2016). Therefore, the design of the frame core-tube structure with PS-SCED braces is helpful to achieve the earthquake-resilient performance.

Fig. 17 further compares the hysteretic responses of the BRB and PS-SCED brace at the forth story. As for the asymmetric deformation in tension and compression of components in the structures, the PS-SCED brace has more energy dissipation in tension than compression and the BRB shows a slightly larger elongation than compression. However, both the two braces present stable energy dissipation capability. The BRB cannot move back to its original position after the load is removed, resulting in a significant large residual drift, as shown in Fig. 17. This behavior can be overcome by using the PS-SCED brace to provide restoring forces to the braced structure, and the residual displacement of the PS-SCED brace can be ignored after unloading. The results indicate that severe damage is accumulated in the BRBs with large residual deformation after earthquakes, while the PS-SCED brace can restore to the initial position.

5. Conclusions

This paper presents the mechanics, tests, and finite element analysis of the PS-SCED brace that employs the friction devices to dissipate seismic energy and the self-centering devices to provide restoring force. The PS-SCED brace is proved to have stable energy dissipation and good self-centering capabilities through low cyclic reversed loading tests. The flag-shaped hysteresis constitutive model for PS-SCED brace is developed, and the comparisons between the test and simulation results demonstrate that this constitutive model can well simulate the experimental mechanical behaviors of the PS-SCED brace. The comparative analyses of seismic responses are

also conducted on the RC frame core-tube structures with PS-SCED braces and BRBs. Results indicate that the two buildings have similar inter-story drift ratio and peak acceleration under frequent earthquakes. Under rare earthquakes, the peak acceleration, base shear force and residual drifts of the structure with PS-SCED braces are smaller than the structure with BRBs. The structure with PS-SCED braces is helpful to achieve the earthquake-resilient performance.

Acknowledgments

The writers gratefully acknowledge the partial support of this research by the National Natural Science Foundation of China under Grant No. 51578058, and Beijing Natural Science Foundation under Grant No. 8172038.

References

Chou, C.C., Chen, Y.C., Pham, D.H. and Truong, V.M. (2014), "Steel braced frames with dual-core SCBs and sandwiched BRBs: Mechanics, modeling and seismic demands", *Eng. Struct.*, **72**, 26-40.

Chou, C.C. and Chen, Y.C. (2015), "Development of steel dual-core self-centering braces: quasi-static cyclic tests and finite element analyses", *Earthq. Spectra*, **31**(1), 247-272.

Christopoulos, C., Pampanin, S. and Priestley, M.J.N. (2003), "New damage index for framed systems based on residual deformations: part I", *J. Earthq. Eng.*, **7**(1), 79-118.

Christopoulos, C., Tremblay, R., Kim, H.J. and Lacerte, M. (2008), "Self-centering energy dissipative bracing system for the seismic resistance of structures: development and validation", *J. Struct. Eng.*, **134**(1), 96-107.

Deierlein, G., Krawinkler, H., Ma, X., Eatherton, M., Hajjar, J., Takeuchi, T., Kasai, K. and Midorikawa, M. (2011), "Earthquake resilient steel braced frames with controlled rocking and energy dissipating fuses", *Steel Constr.*, **4**(3), 171-175.

Eatherton, M., Hajjar, J., Ma, X., Krawinkler, H. and Deierlein, G. (2010), "Seismic design and behavior of steel frames with controlled rocking-part I: concepts and quasi-static subassembly testing", *Proceedings of the ASCE Structures Congress*, Orlando, Florida, USA, May.

Erochko, J., Christopoulos, C., Tremblay, R. and Choi, H. (2010), "Residual drift response of SMRFs and BRB frames in steel buildings designed according to ASCE 7-05", *J. Struct. Eng.*, **137**(5), 589-599.

Han, L.H., Zhao, X.L. and Tao, Z. (2001), "Tests and mechanics model of concrete-filled SHS stub columns, columns and beam-columns", *Steel. Compos. Struct.*, **1**(1), 51-74.

Henry, R.S., Sritharan, S. and Ingham, J.M. (2016), "Residual drift analyses of realistic self-centering concrete wall systems", *Earthq. Struct.*, **10**(2), 409-428.

Hitaka, T. and Sakino, K. (2008), "Cyclic tests on a hybrid coupled wall utilizing a rocking mechanism", *Earthq. Eng. Struct. D.*, **37**(14), 1657-1676.

Liu, Q.Z. and Jiang, H.J. (2017), "Experimental study on a new type of earthquake resilient shear wall", *Earthq. Eng. Struct. D.*, **46**, 2479-2497.

Lu, X.L., Mao, Y.J., Chen, Y., Liu, J.J. and Zhou, Y. (2013), "New structural system for earthquake resilient design", *J. Earthq. Tsunami*, **7**(3), 1350013.

Lu, X.L., Dang, X.L., Qian, J., Zhou, Y. and Jiang, H.J. (2017), "Experimental Study of Self-Centering Shear Walls with Horizontal Bottom Slits", *J. Struct. Eng.*, **143**(3), 04016183.

Lu, X.Z., Lu, X., Guan, H., Zhang, W.K. and Ye, L.P. (2013), "Earthquake-induced collapse simulation of a super-tall mega-braced frame-core tube building", *J. Constr. Steel Res.*, **82**, 59-71.

Mayes, R.L., Brown, A.G. and Pietra, D. (2012) "Using seismic isolation and energy dissipation to create earthquake-resilient buildings", *Bull. New Zealand Soc. Earthq. Eng.*, **45**(3), 117-122.

Miao, Z.W., Ye, L.P., Guan, H. and Lu, X.Z. (2011), "Evaluation of modal and traditional pushover analyses in frame-shear-wall structures", *Adv. Struct. Eng.*, **14**(5), 815-836.
Miller, D.J., Fahnestock, L.A. and Eatherton, M.R. (2012), "Development and experimental validation of a nickel-titanium shape memory alloy self-centering buckling-restrained brace", *Eng. Struct.*, **40**, 288-298.
Miller, D.J., Fahnestock, L.A. and Eatherton, M.R. (2011), "Self-centering buckling-restrained braces for advanced seismic performance", *Proceedings of Structures Congress*, Las Vegas, Nevada, USA, April.
Pampanin, S., Christopoulos, C. and Priestley, M.J.N. (2003), "New damage index for framed systems based on residual deformations: Part II", *J. Earthq. Eng.*, **7**(1), 119-140.
Steele, T.C. and Wiebe, L.D.A. (2017), "Collapse risk of controlled rocking steel braced frames with different post-tensioning and energy dissipation designs", *Earthq. Eng. Struct. D.*, **46**, 2063-2082.
Takewaki, I., Moustafa, A. and Fujita, K. (2012), "Improving the earthquake resilience of buildings: the worst case approach", *Springer Science & Business Media*, New York, USA.
Tremblay, R., Lacerte, M. and Christopoulos, C. (2008), "Seismic response of multistory buildings with self-centering energy dissipative steel braces", *J. Struct. Eng.*, **134**(1), 108-120.
Wu, C.L., Loh, C.H., Yang, Y.S. and Lin, C.H. (2004), "Consideration of collapse and residual deformation in reliability-based performance evaluation of buildings", *Proceedings of the 13th World Conference on Earthquake Engineering*, Vancouver, Canada, August.
Wada, A., Qu, Z., Ito, H. and Motoyui, S. (2009), "Seismic retrofit using rocking walls and steel dampers", *Proceedings of ATC/SEI Conference on Improving the Seismic Performance of Existing Buildings and Other Structures*, San Francisco, California, USA, December.
Xu, L.H., Fan, X.W., Lu, D.C. and Li, Z.X. (2016a), "Hysteretic behavior studies of self-centering energy dissipation bracing system", *Steel Compos. Struct.*, **20**(6), 1205-1219.
Xu, L.H., Fan, X.W. and Li, Z.X. (2016b), "Development and experimental verification of a pre-pressed spring self-centering energy dissipation brace", *Eng. Struct.*, **127**, 49-61.
Xu, L.H., Fan, X.W. and Li, Z.X. (2016c), "Cyclic behavior and failure mechanism of self-centering energy dissipation braces with pre-pressed combination disc springs", *Earthq. Eng. Struct. D.*, **46**(7), 1065-1080.
Xu, L.H., Fan, X.W. and Li, Z.X. (2017), "Experimental behavior and analysis of self-centering steel brace with pre-pressed disc springs", *J. Constr. Steel Res.*, **139**, 363-373.
Xu, L.H., Yan, X.T. and Li, Z.X. (2018a), "Development of BP-based seismic behavior optimization of RC and steel frame structures", *Eng. Struct.*, **164**, 214-229.
Xu, L.H., Xie, X.S. and Li, Z.X. (2018b), "Development and experimental study of a self-centering variable damping energy dissipation brace", *Eng. Struct.*, **160**, 270-280.

TY